JOURNAL OF THE ROYAL SOCIETY Interface

J. R. Soc. Interface (2012) **9**, 1131–1143
doi:10.1098/rsif.2011.0690
Published online 14 December 2011

Air motion sensing hairs of arthropods detect high frequencies at near-maximal mechanical efficiency

Brice Bathellier[1,2,*], Thomas Steinmann[3], Friedrich G. Barth[2,†] and Jérôme Casas[3,†]

[1]*Department of Circuit Neuroscience, Institute for Molecular Pathology (IMP), Dr Bohr-Gasse 7, 1030 Vienna, Austria*
[2]*Department of Neurobiology, Life Sciences, University of Vienna, Althanstrasse 14, 1090 Vienna, Austria*
[3]*Faculté des Sciences et Techniques, Institut de Recherche sur la Biologie de l'Insecte—UMR CNRS 6035, Université François Rabelais, Parc de Grandmont Avenue Monge, 37200 Tours, France*

Using measurements based on particle image velocimetry in combination with a novel compact theoretical framework to describe hair mechanics, we found that spider and cricket air motion sensing hairs work close to the physical limit of sensitivity and energy transmission in a broad range of relatively high frequencies. In this range, the hairs closely follow the motion of the incoming flow because a minimum of energy is dissipated by forces acting in their basal articulation. This frequency band is located beyond the frequency at which the angular displacement of the hair is maximum which is between about 40 and 600 Hz, depending on hair length (Barth *et al.* [1] *Phil. Trans. R. Soc. Lond. B* **340**, 445–461 (doi:10.1098/rstb.1993.0084)). Given that the magnitude of natural airborne signals is known to decrease with frequency, our results point towards the possible existence of spectral signatures in the higher frequency range that may be weak but of biological significance.

Keywords: filiform hairs; airborne signals; sensory physiology; trichobothria; mechanoreceptors

1. INTRODUCTION

The detection of airborne signals is essential for the survival of many arthropods. In numerous species, long and thin hairs responding to airflow are found on various parts of the body. The variety of ethological situations in which these filiform hairs may be useful for the animals is large [2]. They play a critical role in the ability to escape from approaching predators. This was established for the hairs present on the cercus, an antenna-like appendage at the end of many insects such as crickets, cockroaches, mantids and members of several primitive insect families. It is also known that some arthropods such as hunting spiders use airborne signals to detect prey [3–5]. Despite some findings of general significance [6–8], the question as to which features of airborne signals are recognized by the animal to trigger and guide such behaviours clearly needs further attention.

Because of their crucial role, flow-sensitive hairs are likely to have been submitted to strong selective pressures during evolution, which renders them interesting for a study of mechanical optimization. While it is impossible to evaluate all selection forces that have acted on the design of a sensor, a reverse-engineering analysis pinpointing the range of airflows that filiform hairs are best designed to capture will be informative with regard to some of the important features of biologically relevant airflows. Such an analysis is all the more attractive because the physics of arthropod filiform hairs has been well studied in the past and the main features of their mechanical and hydrodynamic design[1] are now well established [9–12].

The extent to which filiform hairs are mechanically optimized is a question that has been often asked in the literature, but the mechanical limits of a hair have never been precisely defined. Shimozawa *et al.* [12] suggested that cricket filiform hairs are optimized to transmit the maximum amount of energy from the shaft of the hair to the receptor neurons located at the basal articulation. This conclusion was based on their observation that the friction of the hair shaft in air and at its basal articulation are balanced, which is a mechanical feature known as impedance-matching and ensures optimal energy transmission. While this observation could, in principle, explain the extreme sensitivity of filiform hairs, which can detect air movement

*Author for correspondence (brice.bathellier@normalesup.org).
†These authors contributed equally to the study.

Electronic supplementary material is available at http://dx.doi.org/10.1098/rsif.2011.0690 or via http://rsif.royalsocietypublishing.org.

[1]'Design' is used in this paper as it is in engineering.

Received 9 October 2011
Accepted 24 November 2011

down to 1 Å [10,13], the range of frequencies for which impedance-matching occurs was not determined in this study. Thus, the particular airflow signals for which the animal might benefit from this particular optimization of the mechanical design are unknown.

In this study, we derived an original, more compact and physically intuitive solution to the general equation of motion, which solves a number of vexing problems and inherent inaccuracies that have plagued the modelling of filiform hairs. Our solution allows the upper limits of physically possible energy transmission and the motion amplitude in any typical filiform hair to be identified in a more straightforward way than with previous approaches. These limits represent benchmarks from which we can assess the degree of mechanical optimization of a hair. Applying these results to optical and particle image velocimetry (PIV)-based measurements of cricket and spider filiform hairs, we observed consistently in both species: (i) that filiform hair dynamics are close to the physical limits only in a specific frequency band and (ii) that this frequency band is beyond the frequency at which the angular displacement of the hair is maximal. So far, this frequency has been considered to be the most representative of the type of airflows for which filiform hairs have evolved. Because our results show that the design of filiform hairs has actually been constrained to mechanically optimize the reception of higher frequencies, they call for reconsidering this idea.

Existing studies suggest that the power spectra of ethologically relevant and background biological airflows are dominated by relatively low frequencies [7,8,14], which therefore constitute the range of signals that are easiest to capture. By revealing an unsuspected mechanical optimization of filiform hair receptors in the frequency range higher than that of maximum angular deflection, our study points towards the existence of spectral signatures that may be weak, but have been sufficiently relevant to maintain evolutionary pressure on the hair's mechanical properties. A number of studies have already suggested that higher frequency components and transients in airflows are important cues making a distinction between background flows and biologically relevant signals possible [3,14,15]. At the end of this paper, we discuss how far an approaching object, being a prey or a predator, actually generates such signatures.

2. MATERIAL AND METHODS

2.1. Hair model

Our mathematical model of filiform hairs is essentially the model introduced by Humphrey *et al.* [11] but derived in a more general way. The hair is viewed as a straight cylinder of length L and diameter d, standing vertically on a flat plate and rotating around its base. The joint linking the hair to the cuticle is modelled as a linear viscoelastic element that resists hair deflection θ with a torque $-S\theta$ and also applies a frictional torque $-R(\mathrm{d}\theta/\mathrm{d}t)$, which reflects the rotational energy dissipated by the hair in the joint (figure 1). It should be noted that this description does not account for viscoelasticity effects in the articulation. Such effects were observed in spider trichobothria [16] but for very low angular velocities (less than 0.05 rad s^{-1}). Because the angular velocities considered in this study are much higher (greater than 10 rad s^{-1}), we neglected these effects. The hair is displaced by a far-field horizontal sinusoidal flow $v(t) = U\cos(\omega t)$ in a fluid of density ρ and viscosity μ, where f is the frequency of the oscillation and $\omega = 2\pi f$. As shown by Humphrey *et al.* [11], the fluid is slowed down by viscous forces as it approaches the substrate to which the hair is attached, so the velocity $v(z,t)$ of the air flow arriving on the hair depends on the vertical position z (figure 1*a*). Biologically relevant airflows are generally relatively slow ($U < 1$ m s^{-1}) and the diameter of arthropod filiform hairs is small (approx. 10 µm). Hence, airflows around filiform hairs are characterized by low Reynolds numbers ($Re = U\rho d/\mu$; see Humphrey *et al.* [11] for details) which implies a laminar flow behaviour (absence of turbulence induced by the hair). Moreover, at low Reynolds numbers, the equations describing the motion of the fluid become linear to a very good approximation, and the force exerted on the perturbing object (here the hair) changes linearly with the relative velocity of the fluid and its derivative [17].

An element of hair of length $\mathrm{d}z$ and moving at speed $v_{\mathrm{hair}}(z,t)$ is subject to a force

$$\mathrm{d}F(z,t) = \left(\rho\pi\frac{d^2}{4}\frac{\partial(v(z,t)-v_{\mathrm{hair}}(z,t))}{\partial t} + \alpha(v(z,t)-v_{\mathrm{hair}}(z,t))\right)\mathrm{d}z. \tag{2.1}$$

The first term on the right-hand side of the equation corresponds to the amount of linear momentum given to the fluid that is displaced by the hair when it moves. The second term is the viscous drag exerted on the hair, with α being the drag coefficient of the hair. For a low-density fluid such as air and for frequencies up to 1000 Hz, we computed that the first term contributes less than 1 per cent of the total force and can be neglected (see also [11,18]).

As for the second term, there exists no general expression for the drag coefficient. Estimations of α have been calculated using different approximations. In studies of arthropod filiform hairs, two approximations have been considered so far.

— Neglecting the unsteady acceleration term in the Navier–Stokes equation leads to the Oseen drag coefficient in the medium $\alpha = 16\pi\mu/(\ln(8\mu/d\rho U) - 0.154)$, which does not depend on oscillation frequency [12].
— Neglecting the convective acceleration term leads to Stokes' drag coefficient $\alpha = \pi\mu G(4 - \mathrm{i}\pi/g)$ with $G = -g/(g^2 + \pi^2/16)$ and $g = 0.577 + \ln(d/4\sqrt{\omega\rho/\mu})$. Stokes' drag depends weakly on both hair diameter and oscillation frequency [1,11,12].

Mathematically, neither of these approximations fully applies to the problem of arthropod filiform hairs and it is likely that the value of the actual drag coefficient lies

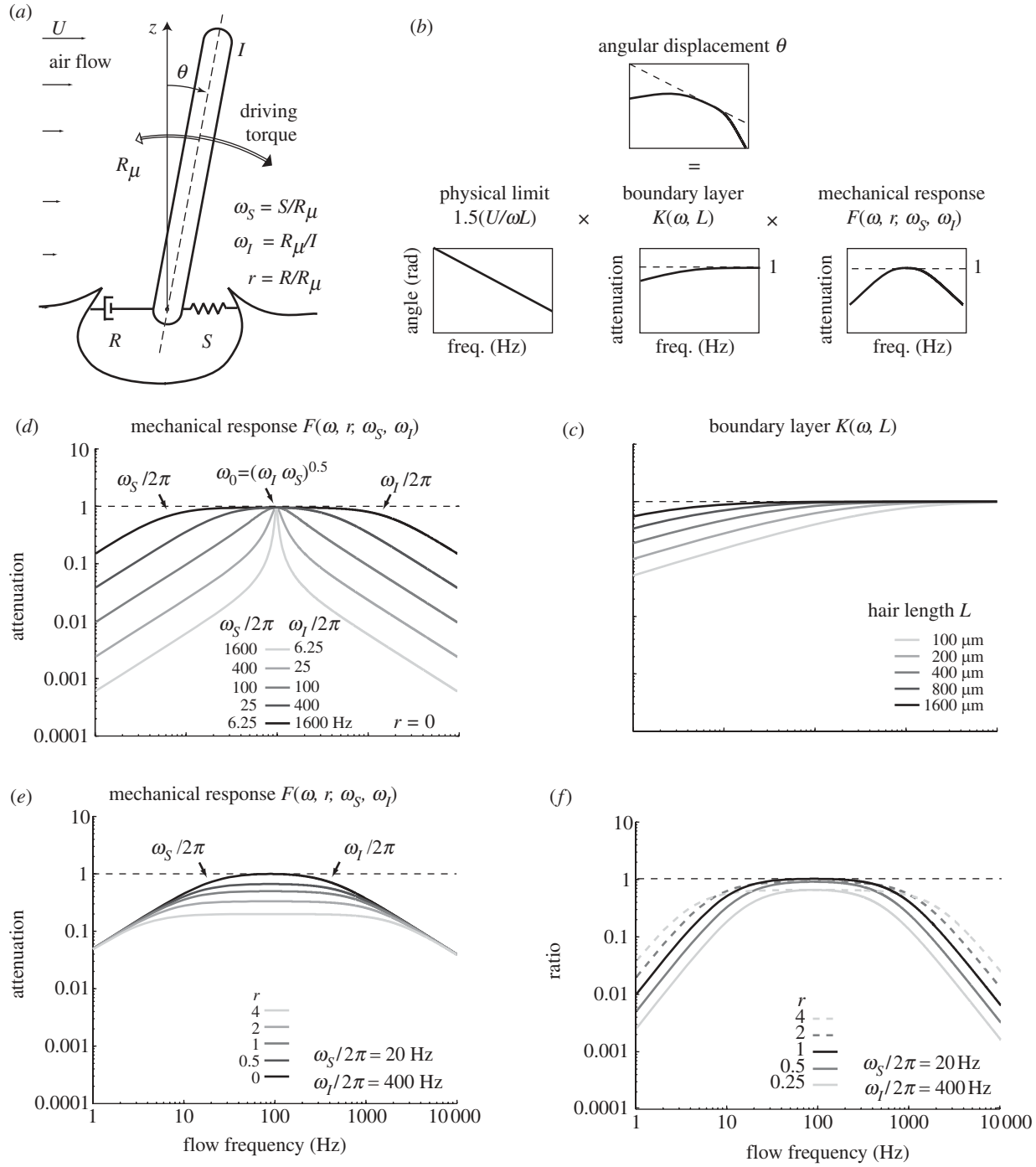

Figure 1. The components of filiform hair dynamics. (*a*) General model of a filiform hair (see text for details). (*b*) The frequency response of a filiform hair can be decomposed as the product of three components: the maximum possible response; the effect of the boundary layer close to the substrate on which the hair is standing; and the mechanical response of the hair. (*c*) The boundary layer effect on filiform hairs of different lengths for a flow over an infinite planar substrate. (*d*) The mechanical response function for hairs having the same natural frequency $\omega_0 = (\omega_I\omega_S)^{0.5}$ but different width of tuning through the choice of different reduced restoring and inertial constants ω_S and ω_I (light grey to black: resonant to over-damped response). The reduced damping constant r is set here to 0. (*e*) Mechanical response function for different values of r. (*f*) Ratio of energy actually transmitted to the basal articulation to the maximum possible transmitted energy for a hair of given length and diameter. The maximum possible energy transmission is reached at the natural frequency for $r = 1$ (impedance-matching).

somewhere in between these two extremes cases (see details in the electronic supplementary material). However, because Oseen's drag force does not depend on frequency and Stokes' does so only weakly, α can for any case be well-approximated as a constant, which suffices to describe the physics of all studied filiform hairs.

For low angular displacements, we can approximate linearly $v_{\mathrm{hair}}(z,t) = z(\mathrm{d}\theta/\mathrm{d}t)$. Then, the torque exerted by the fluid on the filiform hair is

$$T(t) = \alpha \int_0^L z\left(v(z,t) - z\frac{\mathrm{d}\theta}{\mathrm{d}t}\right)\mathrm{d}z. \qquad (2.2)$$

Applying the conservation of angular momentum for the hair leads to the equation of hair motion

$$I\frac{\mathrm{d}^2\theta}{\mathrm{d}t^2}+R\frac{\mathrm{d}\theta}{\mathrm{d}t}+S\theta=T, \tag{2.3}$$

where I is the moment of inertia of the hair.

2.2. Solution of the equation of motion

The linearity of the equations of hair motion allows us to assume that the angular displacement of the hair will be of the form $\theta(t)=\theta_{\max}\cos(\omega t-\phi)$, where $\theta_{\max}$ is the maximum amplitude of the deflection and ϕ its phase shift relative to far-field air motion. For reason of simplicity, we use the complex notation in which we write $\theta(t)=\theta_{\max}(\omega)\exp(\mathrm{i}\phi(\omega))\exp(\mathrm{i}\omega t)$. Thus, time-derivatives of complex quantities can be more easily computed, which is a substantial practical advantage: $\mathrm{d}\theta/\mathrm{d}t=\mathrm{i}\omega\theta$ and $\mathrm{d}^2\theta/\mathrm{d}t^2=-\omega^2\theta$. In this notation, the real physical quantity is the real part of its associated complex quantity. For the sake of generality, we must assume that the coefficient of friction is a complex number $\alpha=|\alpha|\exp(-\mathrm{i}\phi_\alpha)$ because we cannot exclude the existence of a phase shift between air velocity and the force as seen in Stokes' drag coefficient. However, we obtained more accurate results with $\phi_\alpha=0$, as in Oseen's drag coefficient (see details in the electronic supplementary material) and, therefore, we used $\phi_\alpha=0$ in all results presented in this paper. The velocity of the airflow arriving on the hair can also be written in a very general way as $v(z,t)=Uk(\omega, z)\exp(\mathrm{i}\omega t)$, where $k(\omega, z)$ is a complex function representing the amplitude and phase of air velocity along the vertical axis. Typically, k will depend on the geometry of the substrate to which the hair is attached [11].

Introducing the complex notation in equation (2.3) and moving all terms dependent on θ to the left-hand side, the equation of motion becomes

$$\begin{aligned}&-\omega^2 I\theta(t)+\mathrm{i}\omega\left(R+\alpha\int_0^L z^2\mathrm{d}z\right)\theta(t)+S\theta(t)\\&=\alpha U\exp(\mathrm{i}\omega t)\int_0^L zk(\omega,z)\mathrm{d}z.\end{aligned} \tag{2.4}$$

Computing the integral on the left-hand side, we obtain the frictional term representing the damping of hair motion by the fluid. It is *a priori* a complex number that we write $\alpha\int_0^L z^2\mathrm{d}z=R_\mu+\mathrm{i}R_\mu^*$ with $R_\mu=(L^3/3)|\alpha|\cos(\phi_\alpha)$ and $R_\mu^*=-(L^3/3)|\alpha|\sin(\phi_\alpha)$. In the integral of the velocity profile, we change z into $x=z/L$ and we define the function

$$\begin{aligned}K(\omega,L)&=|K(\omega,L)|\exp(-\mathrm{i}\phi_K)\\&=2\int_0^1 xk(\omega,xL)\mathrm{d}x.\end{aligned} \tag{2.5}$$

Then, we have $\alpha\int_0^L zk(\omega,z)\mathrm{d}z=\alpha L^2K(\omega,L)/2=3(R_\mu+R_\mu^*)K(\omega,L)/2L$. Finally, we obtain from (2.4) the complex solution for θ (note that the time-dependence $\exp(\mathrm{i}\omega t)$ is dropped because it is present on both sides of the equation):

$$\begin{aligned}&\theta_{\max}(\omega)\exp(-\mathrm{i}\phi(\omega))\\&=\frac{3U}{2L}\frac{1}{\mathrm{i}\omega}\frac{\mathrm{i}\omega\left(R_\mu+\mathrm{i}R_\mu^*\right)}{S-\omega^2I+\mathrm{i}\omega(R+R_\mu+\mathrm{i}R_\mu^*)}K(\omega,L).\end{aligned} \tag{2.6}$$

One very important aspect of the physics of filiform hairs is that the friction of air on the hair shaft yields both a driving and a dissipative torque, which can cancel each other. The mathematical consequence is that the air-damping torque ($\mathrm{i}\omega R_\mu$) appears both in the numerator and denominator in equation (2.6). To best capture this aspect of filiform hair physics, it is convenient to divide the numerator and denominator by $\mathrm{i}\omega R_\mu$ and to introduce the reduced mechanical constants $\omega_S=S/R_\mu$, $\omega_I=R_\mu/I$ and $r=R/R_\mu$. Finally, we write the deflection as the product of three frequency dependent terms

$$\theta_{\max}(\omega)\exp(-\mathrm{i}\phi(\omega))=\left(\frac{3U}{2L}\frac{1}{\mathrm{i}\omega}\right)F(\omega,r,\omega_S,\omega_I)K(\omega,L) \tag{2.7}$$

with

$$F(\omega,r,\omega_S,\omega_I)=\frac{1-\mathrm{i}\tan\phi_\alpha}{1+r-\mathrm{i}(\omega_S/\omega-\tan\phi_\alpha-\omega/\omega_I)}. \tag{2.8}$$

Taking the modulus of equation (2.7) gives the maximum angular displacement, whereas taking the argument leads to the phase shift between far-field air velocity and hair deflection.

The power dissipated in the basal articulation over a cycle of period $T=1/f$ is given by the integral of the dissipation torque multiplied by the angular velocity $(1/T)\int_0^T R(\mathrm{d}\theta/\mathrm{d}t)^2\mathrm{d}t=(1/2)R(\omega\theta_{\max}(\omega))^2$, which gives equation (3.2) of §3 after replacement with equation (2.7) and changing R into rR_μ.

2.3. Deflection measurements for spider trichobothria

For measurements of deflection dynamics of spider trichobothria, a sinusoidal velocity field was produced by a loudspeaker with its membrane oriented perpendicular to the leg axis and parallel to the long axis of the hair. Air velocity was measured indirectly from pressure gradient $\Delta P_{\max}$ measurements using a movable probe microphone (Bruel & Kjaer Type 4182), which gave the instantaneous local air pressure with high temporal resolution. Pressure gradient is related to velocity via the Navier–Stokes equation, which simplified for a flow oscillating at pulsation $\omega=2\pi f$ gives $U=|\Delta P_{\max}/\omega\rho\Delta x|$ and $\phi_{\text{velocity}}=\phi_{\text{pressure}}+\pi/2$. The microphone was moved in $\Delta x=1$ cm steps along the leg axis. The two measurement points of the pressure gradient were placed symmetrically on each side of the examined hair. Pressure gradient measurements were also performed perpendicular to the leg axis to ensure that the flow was oriented along the leg. Estimates of the error made on the calibration of

the flow were obtained by repeating the calibration procedure several times from its beginning. The maximal velocity of the airflow was obtained with a precision of ± 10 per cent, while the error of its phase was below 5°.

The leg was autotomized from the spider just before measurements began and was glued to a glass pipette (diameter 6 mm) allowing for a continuous injection of a physiological solution to prevent desiccation. We also shaved all the hairs around the trichobothria to improve observation. The hairs were deflected by a constant far-field velocity of 30 mm s^{-1}, with frequencies ranging from 25 to 300 Hz. The maximum angular displacement was measured optically with a binocular microscope (50× objective) coupled to a charge-coupled device (CCD) camera. The maximal angular displacement was deduced from the distance between two extreme positions of the hair at a given height along its length. The phase shift was determined using two stroboscopes flashing with a fixed 180° phase shift. The overall phase of the stroboscopes was varied to make the measurement. In this configuration, the two stroboscopic images of the hair merge when the hair is at the middle of the position signalling precisely the 90° phase of hair deflection.

2.4. Deflection measurements for cricket cercal hairs

Adult female crickets (*Nemobius sylvestris*) were anaesthetized by chilling and their legs, wings and ovipositor were removed. To minimize flow disturbance around the hair of interest, surrounding hairs were carefully plucked using a microdissection forceps. Crickets were fixed on a micromanipulator and placed in a sealed glass box which was filled with air seeded with 200 nm oil particles (diethylhexylsebacat) applied by an aerosol generator. Oscillating airflows were generated by a loudspeaker (40 W) driven by a sine-wave generator.

To measure both far-field airflow and hair-tip velocity, we used a PIV-pulsed laser (NewWave Research Solo PIV 2, 532 nm, 30 mJ, Nd:YAG, dual-pulsed, pulse duration 4 + 1 ns; Dantec Dynamics A/S) producing a thin illumination sheet (width = 17 mm, thickness at focus point = 50 μm). The laser sheet was focalized on a portion of the cricket cercus, providing an illumination of a small cross section including the cercus and the plane of vibration of the isolated hair. The laser was operated at low power (3 mJ at 532 nm wavelength) to minimize glare. The target area was imaged onto the CCD array of a digital camera (696 × 512 pixels) with a stereomicroscope to produce a field of view of 2700 × 2000 μm.

Instantaneous particle and hair-tip velocities were deduced from displacements measured by the cross-correlation of a pair of images acquired at 500 μs intervals, synchronously with the laser pulses. According to our evaluations, the absolute precision was 0.8 mm s^{-1} [19]. In all experiments, the far-field flow amplitude was set between 15 and 20 mm s^{-1}. For a 5 μm-diameter hair in air at 20°C, this corresponded to a biologically relevant Reynolds number between 0.05 and 0.07, which is comparable with the values found for flows experienced by a cricket in nature. Acquisition of instantaneous velocities was performed at a rate of 20 Hz but sinusoidal motion could be reconstructed from the knowledge of the phase of every measurement with respect to the flow generator signal (stroboscopic principle, see Steinmann *et al.* [19]).

3. RESULTS

3.1. Physical limits of filiform hair dynamics

The interaction of air with the shaft is well described by a frictional force which grows linearly with air velocity. This frictional force results in a torque that we express as $R_\mu \, \mathrm{d}\theta/\mathrm{d}t$, where $\theta(t)$ is the angular displacement of the hair (figure 1*a*) and R_μ is a constant. The basal articulation is well described by an elastic mechanical element that resists the motion to return the hair back in its equilibrium position, combined with a frictional element which slows down the motion and dissipates its energy. We note the resulting torques as $S\theta(t)$ and $R \, \mathrm{d}\theta/\mathrm{d}t$, respectively (figure 1*a*). Finally, the dynamics of the hair cannot be fully understood without considering the hydrodynamics of the airflow as it approaches the exoskeletal substrate to which the hair is coupled. As shown by others [11,19], the presence of the substrate results in vertical variations in the airflow velocity, which are often referred to as boundary layer effects, and which we also include in the present hair model (figure 1*a*).

Based on this classical description, we derived a closed-form analytical solution for the peak angular displacement $\theta_{\max}$ of a hair oscillating in a sinusoidal air flow. For a filiform hair of length L in an airflow oscillating at frequency f and peak velocity U (note that for clarity, we use the angular frequency $\omega = 2\pi f$ instead of the frequency f in all equations), we have

$$\theta_{\max}(\omega) = \frac{3U}{2L}\frac{1}{\omega}|K(\omega, L)||F(\omega, r, \omega_S, \omega_I)|, \qquad (3.1)$$

where $r = R/R_\mu$, $\omega_S = S/R_\mu$, $\omega_I = R_\mu/I$ are reduced constants and $|F(\omega, r, \omega_S, \omega_I)| = 1/\sqrt{(1+r)^2 + (\omega_S/\omega - \omega/\omega_I)^2}$. Importantly, we used the complex notation instead of an explicit description of the time-dependencies with sine functions to obtain more compact and, therefore, more physically intuitive mathematical expressions than previous studies. Furthermore, peak angular velocity or acceleration can be straightforwardly obtained by multiplying $\theta_{\max}(\omega)$ by ω or ω^2 in the complex notation. The reduced constants also ease the physical understanding of the system because they summarize the competition between different forces acting on the hair to determine its response. Here, we have chosen them as ratios of the intrinsic mechanical constants of the hair to its effective damping coefficient in the fluid (R_μ). Hence, the reduced constants set the conditions for the forces acting on the hair to be smaller or bigger than the damping in air.

While $\theta_{\max}(\omega)$ describes the sensitivity of the motion of the hair shaft itself, it is also important to know how much energy is available for the transduction of hair motion into nervous signals by the underlying sensory

neurons, which in our framework corresponds to the energy dissipated in the basal articulation [12]. Indeed, the biochemical processes responsible for the signal transduction must have some energy barriers, which will limit the transduction of very small signals [20]. The energy dissipated over an oscillation cycle of the airflow derives from $\theta_{\max}(\omega)$. Here, we express it as the energy per unit of time (i.e. power) to allow for comparisons between different flow frequencies:

$$\frac{E_R(\omega, T)}{T} = \frac{3U^2|\alpha|L}{32}|K(\omega, L)|^2|2\sqrt{r}F(\omega, r, \omega_S, \omega_I)|^2, \tag{3.2}$$

where $|\alpha|$ is the friction coefficient (per unit of length) of air on the hair shaft (see §2).

The main novelty of equations (3.1) and (3.2) is that they give the angular displacement and the dissipated energy as products of three terms (figure 1*b*), each of which accounts for a distinct physical process. The terms $|F(\omega, r, \omega_S, \omega_I)|$ and $|2\sqrt{r}F(\omega, r, \omega_S, \omega_I)|^2$ summarize the influence of the mechanics of the basal articulation on motion and energy transmission, respectively. Both are normalized such that they are unitless and their values are always between 0 and 1 (figure 1*d*). The term $|K(\omega, L)|$ summarizes the influence of the substrate on the incoming flow (boundary layer). It is also unitless. In common situations like that of a flat (as in figure 1*c*) or a cylindrical substrate with the flow oriented parallel to the surface and the cylinder's long axis (electronic supplementary material, figure S1), the flow is decelerated by the substrate. In these cases, values for $|K(\omega, L)|$ are strictly between 0 and 1. In particular cases, the flow is locally accelerated by the substrate and $|K(\omega, L)|$ can become slightly larger than 1 (e.g. flow transverse to a cylindrical substrate, see the electronic supplementary material, figure S1). However, because we are interested in the optimization of the intrinsic mechanical properties of the hair, we focus on the response of the hair corrected for the influence of the boundary layer, which we consider as an independent pre-filtering stage. In our framework, this correction is straightforward and simply consists of dividing angular displacement and transmitted energy by $|K(\omega, L)|$ and $|K(\omega, L)|^2$, respectively.

In that case, because $|F(\omega, r, \omega_S, \omega_I)|$ and $|2\sqrt{r}F(\omega, r, \omega_S, \omega_I)|^2$ are always smaller than or equal to 1, the first terms of equations (3.1) and (3.2) represent the maximum angular displacement and the maximum transmitted energy, respectively, that a hair of a given length can ever reach, regardless of the mechanical parameters of its articulation. Thus, the physical limits for angular displacement and energy transmission are

$$\theta_{\text{limit}}(\omega) = \frac{3U}{2L}\frac{1}{\omega} \tag{3.3}$$

and

$$\left.\frac{E_R(\omega, T)}{T}\right|_{\text{limit}} = \frac{3U^2|\alpha|L}{32}. \tag{3.4}$$

These limits represent important benchmarks that we can use to assess the degree of mechanical optimization of real filiform hairs. It is noteworthy that while the limit for transmitted energy is independent of frequency, the limit for angular displacement decreases with frequency. This reflects the simple fact that, at constant peak velocity (or equivalently at constant airflow energy), the peak-to-peak displacement of air particles must decrease with increasing flow frequency.

3.2. Conditions to reach the physical limits

Now that we have identified the physical limits of angular displacement and energy transmission, we can ask which mechanical properties of the hair sensillum allow these limits to be reached. In our framework, this question can be answered by analysing the behaviour of the function $|F|$ as we vary the mechanical parameters of the hair. This analysis is relatively straightforward because $|F|$ has the typical mathematical structure of a second-order linear oscillator

$$|F(\omega, r, \omega_S, \omega_I)| = \frac{1}{\sqrt{(1+r)^2 + (\omega_S/\omega - \omega/\omega_I)^2}}. \tag{3.5}$$

Physically, $|F|$ represents how much the hair deviates from the largest possible motion owing to its inertia and to the forces in the basal articulation that resist hair motion. Each term in the denominator of equation (3.5) represents the influence of a particular force acting on the hair. The ratio ω_S/ω represents the elastic force exerted at the base of the hair. For any choice of parameter, this term becomes dominant in the lower frequency range ($|F(\omega, r, \omega_S, \omega_I)| \sim (\omega/\omega_S)$ for $\omega \to 0$), which means that elastic forces always prevent filiform hair motion from reaching its limit at lower frequencies (figure 1*d*). The symmetric term ω/ω_I represents the inertia of the hair and always becomes dominant at higher frequencies ($|F(\omega, r, \omega_S, \omega_I)| \sim (\omega_I/\omega)$ for $\omega \to \infty$). Thus, inertia always prevents the hair from reaching the physical limit as shown in figure 1*d* at higher frequencies. It is noteworthy that the effects of inertia and elastic forces grow with $1/\omega$ and ω, implying that they influence the motion of a hair more strongly than the boundary layer effects ($|K|$), which typically grow as $\sqrt{\omega}$ (compare figure 1*c*,*d*).

Between these two extremes, $\omega \to 0$ and $\omega \to \infty$, $|F|$ passes through a single maximum $1/\sqrt{(1+r)^2}$ at the natural frequency $f_0 = \sqrt{\omega_S\omega_I}/2\pi = \sqrt{S/I}/2\pi$. Depending on the damping ratio $\zeta = (1+r)\sqrt{\omega_I/\omega_S}/2$, this maximum can be sharp, in which case the hair is resonant ($\zeta < 1$, e.g. figure 1*d*, light grey curves), or is located in the centre of a broad plateau, in which case the hair is over-damped ($\zeta > 1$; figure 1*d*, black curve). In the latter situation, the hair has three distinct dynamical regimes covering three distinct frequency regions. Frequencies for which elastic forces dominate ($\omega < \omega_S$) are followed by a band where only damping forces dominate ($\omega_S < \omega < \omega_I$) and finally for $\omega > \omega_I$, inertial forces dominate.

Hence, there are two conditions for a hair to reach its physical limit for angular displacement: (i) the flow

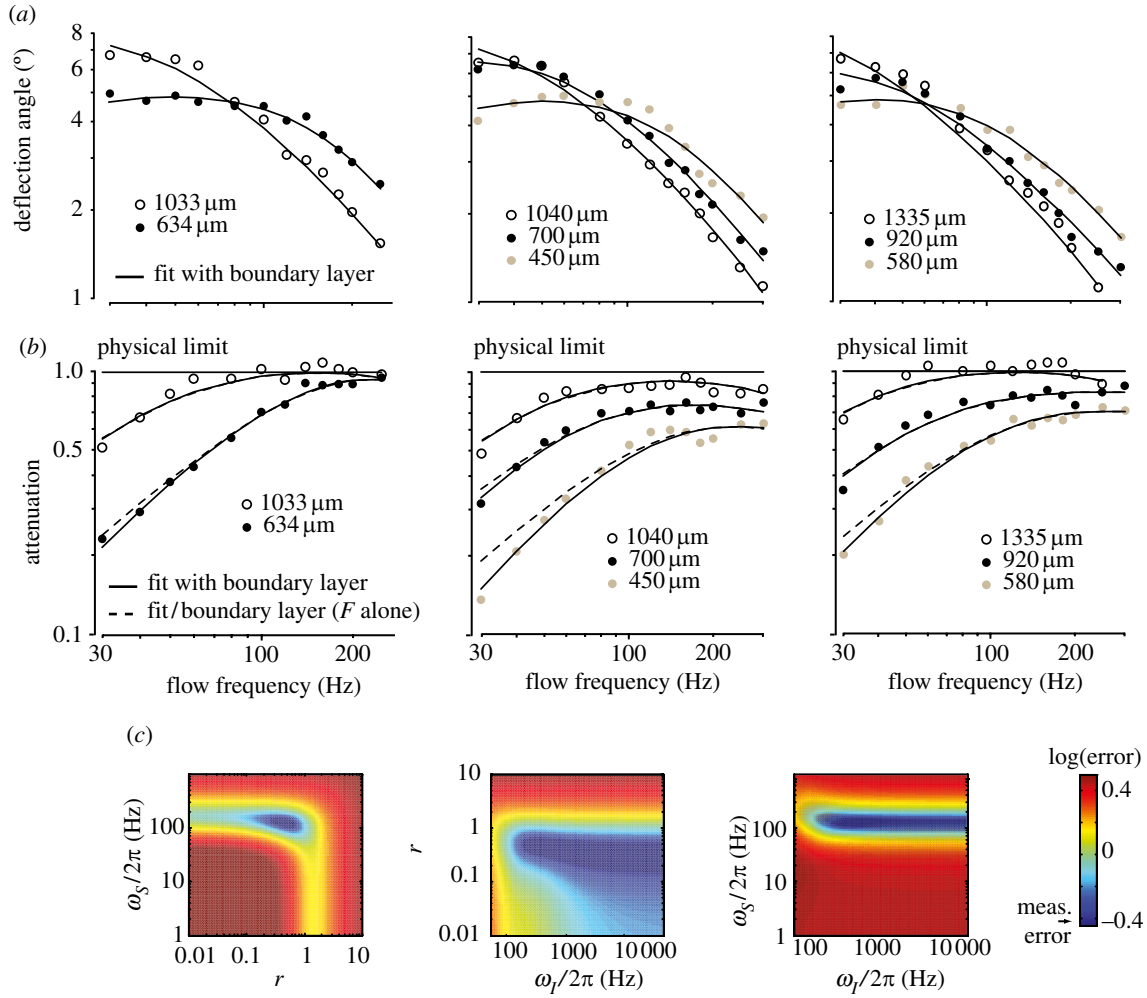

Figure 2. Measurements of filiform hair motion in the spider *Cupiennius salei*. (*a*) Measurements of the peak angular displacement of eight spider trichibothria at different flow frequencies. (*b*) Deviation from the physical limit calculated by dividing the angular displacement of the hair by its physical limit (equation (3.3)) for the same trichobothria as in (*a*). Solid lines: best fit to $|F(\omega,r,\omega_S,\omega_I)\,K(\omega,L)|$ (fitted parameters r, ω_S, ω_I are given in table 1), where F is defined as in equation (2.8) and K is obtained from the equation of the flow parallel to a cylinder (i.e. approximation of the cercus). Dashed lines: estimation of $|F(\omega,r,\omega_S,\omega_I)|$ alone. (*c*) Precision of the determination of fitted parameters for one of the spider trichobothria ($L = 580\,\mu$m). The maps represent the mean error between the model and the data made for different pairs of mechanical parameters. Only r, ω_S can be accurately determined, while a large range of ω_I values yield a fitting error within the measurement error (blue range).

frequency should be at its natural frequency f_0, where the sum of inertial and elastic forces becomes negligible ($\omega_S/2\pi f_0 - 2\pi f_0/\omega_I = 0$) and (ii) the maximum of function $|F|$ (or $|2r\,F^2|$, respectively) should be equal to 1. Therefore, the largest possible motion is reached at f_0 when $r \to 0$, that is, when damping in the articulation becomes negligible with respect to damping in air (figure 1*e*). Interestingly, in the latter situation, only hydrodynamic forces are effectively driving and damping the hair, so that most of its energy is dissipated in the medium itself. In that case, one can consider that the hair follows the motion of the flow as closely as possible.

Likewise, the largest possible energy transmission is also reached at f_0 when $r = 1$ (figure 1*f*), that is when damping in air and in the basal articulation are balanced. This situation corresponds to impendence-matching as shown by Shimozawa *et al.* [12]. However, here we show that impedance-matching can be achieved only near the natural frequency, which was overlooked in the latter study.

This new theoretical observation that a filiform hair is mechanically optimal only near its natural frequency raises two questions. First, what is the actual range of frequencies where real filiform hairs are closest to their mechanical optima? Second, are filiform hairs working closer to the physical limit of energy transmission, as suggested by Shimozawa *et al.* [12], or alternatively closer to the physical limit of motion?

3.3. Frequency range for which cricket and spider hairs approach the physical limit

Motivated by these questions, we measured the deflection of filiform hairs on the leg of the spider *Cupiennius salei* (figure 2) and in the cricket species *N. sylvestris* (figure 3). For spider hair sensilla, we

Table 1. Fitted mechanical constants for spider and cricket hairs with error estimates. This table gives the reduced mechanical constants obtained by fitting our model (equations (3.1) and (3.5)) to the experimental data for all hairs measured in this study. We also estimated the precision of fitted constants by considering all combinations of parameters which yielded a residual error lower than our higher bound estimation of the measurement error as illustrated in figure 2*c*, where an example of a residual error landscape is plotted.

		fitted values				error estimate						
	L (μm)	$\omega_S/2\pi$	r	$\omega_I/2\pi$	ζ	$\omega_{S\min}/2\pi$	$\omega_{S\max}/2\pi$	$r_{\min}$	$r_{\max}$	$\omega_{I\min}/2\pi$	$\omega_{I\max}/2\pi$	$\zeta_{\min}$	$\zeta_{\max}$
Cupiennius salei	450	152	0.61	307	0.44	132	175	0.33	0.76	153	∞	0.29	∞
	580	123	0.43	536	0.73	100	142	0.15	0.61	188	∞	0.40	∞
	634	123	0.08	435	0.87	107	142	0	0.27	176	∞	0.50	∞
	700	76	0.33	406	0.87	57	93	0.15	0.50	188	∞	0.55	∞
	920	66	0.20	1005	1.63	53	81	0.04	0.33	249	∞	0.74	∞
	1033	46	0.00	500	1.62	35	57	0	0.09	249	∞	1.03	∞
	1040	46	0.11	435	1.38	33	61	0	0.23	232	∞	0.92	∞
	1335	33	0.00	466	1.87	22	40	0	0.06	286	∞	1.32	∞
Nemobius sylvestris	410	187	0.81	8738	1.89	142	231	0.53	1.15	267	∞	0.29	∞
	440	123	0.50	6610	2.44	81	163	0.25	0.76	329	∞	0.47	∞
	690	187	0.57	378	0.45	163	231	0.17	0.76	176	∞	0.28	∞
	700	81	0.53	3527	2.15	57	100	0.35	0.75	249	∞	0.53	∞
	870	57	0.13	435	1.22	43	71	0	0.27	249	∞	0.88	∞
	870	142	0.31	50 000	7.19	115	175	0.04	0.66	249	∞	0.42	∞

performed direct optical measurements of peak angular displacement $\theta_{\max}$ (figure 2*a*) from which we computed the deviation from the physical limit based on the far-field airflow velocity measured by a pressure gradient method (electronic supplementary material; §2). For cricket hairs, we used PIV (figure 3*a*,*b*) to directly measure the far-field air velocity U and the velocity of the hair-tip. Dividing the measured angular displacement $\theta_{\max}$ by $3U/(2L\omega)$, we obtained the deviation from its physical limit for each hair (i.e. the product of functions $|K|$ and $|F|$, see equation (3.1)). We also theoretically estimated the influence of the boundary layer $|K|$ to isolate the mechanical response $|F|$ of the hair (figures 2*b* and 3*c*).

We observed, both in the cricket and in the spider, that $|F|$ steadily increases at low frequencies to reach a plateau close to 1 at higher frequencies. This plateau corresponds to the range of frequencies for which filiform hairs are closest to the physical limit of angular displacement and energy transmission, near the natural frequency of the hair. Here, the natural frequency itself was difficult to identify because the width of the plateau was large (filiform hair sensilla are typically over-damped) and the fact that the higher frequency cut-off of the plateau is not seen in our measurements. Most importantly, we observed in all cases that filiform hairs approached their physical limits at frequencies higher than the frequency at which angular displacement was at its maximum (compare figure 2*a* with 2*b*). Therefore, filiform hairs are not mechanically optimized at their maximum angular displacement but are optimized at higher frequencies. This unexpected observation suggests that frequencies beyond the maximum angular displacement of the hairs have a more important role than often thought.

3.4. Estimation of the parameters underlying the mechanical optimization

In order to better understand the mechanical design that leads to the optimization of the filiform hair response at higher frequencies, we estimated the reduced mechanical parameters ω_S, ω_I and r of the hairs (table 1). Reduced parameters allow for direct calculation of the motion, whereas absolute mechanical constants, provided by earlier studies [11,12], require the knowledge of the drag force, which, so far, has only been provided by approximate theories (see §2 and electronic supplementary material). At present, it is therefore more accurate to measure reduced constants. The parameter r which is the ratio of damping (energy dissipation) in the medium and in the articulation was particularly important for finding out whether angular motion or energy transmission is optimized in filiform hairs. Indeed, maximizing energy transmission requires balanced damping in air and in the medium (impedance-matching, $r = 1$), whereas maximizing angular motion requires minimal damping in the articulation ($r \to 0$).

To evaluate these parameters, we fitted equations (3.1) and (3.5) to our measurements (figures 2*b* and 3*c*). The fits were performed by least-squares optimization, exploring all possible combinations of the three parameters

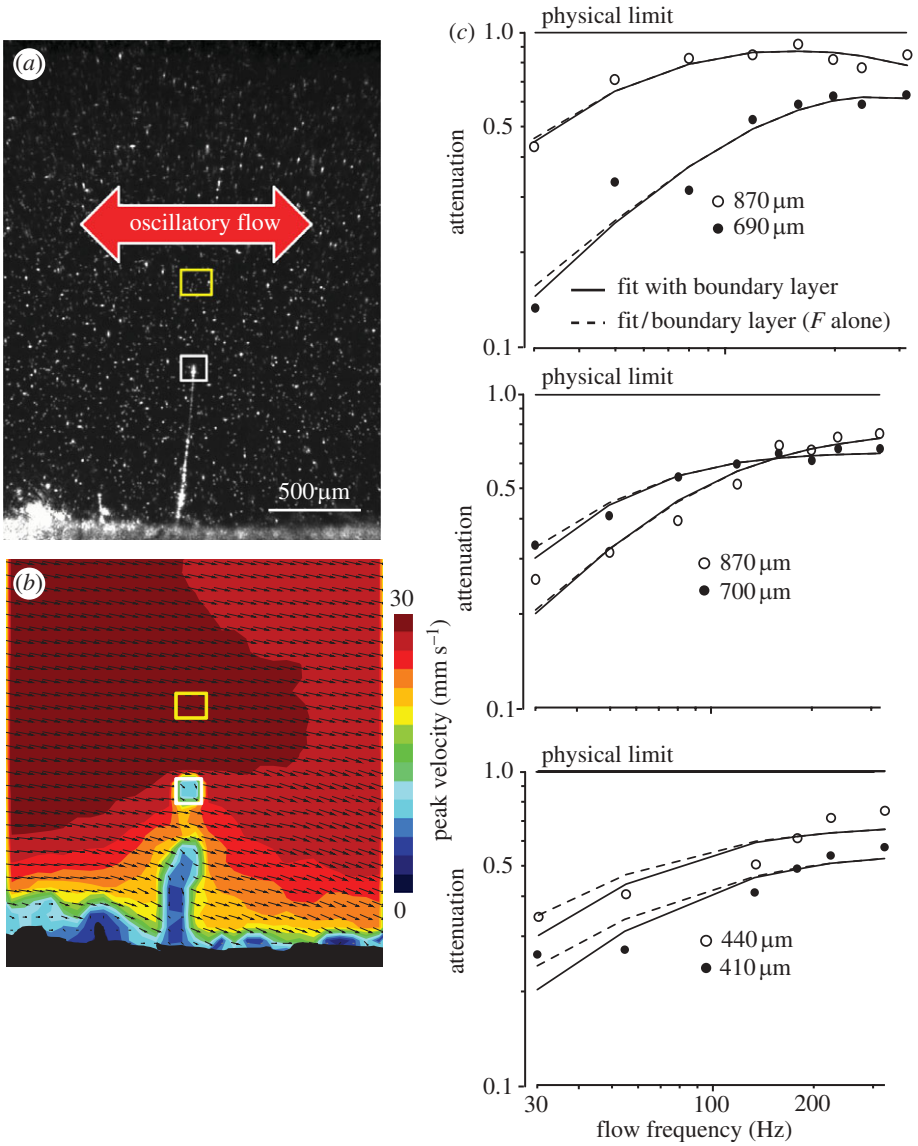

Figure 3. Measurements of filiform hair motion in the cricket *Nemobius sylvestris*. (*a*) Picture of a cricket cercal hair in the particle image velocimetry (PIV) recording chamber. (*b*) Map of instantaneous air particle velocity (colour code) and direction (arrows) measured by the PIV method. The yellow and white squares represent the areas selected to compute far-field flow velocity and hair-tip velocity, respectively. (*c*) Deviation from the physical limit calculated by dividing the tip velocity of the hair measured by PIV by its physical limit (equation (3.3)) for six isolated cricket cercal hairs. Solid lines: best fit to $|F(\omega, r, \omega_S, \omega_I)\ K(\omega, L)|$ (fitted parameters r, ω_S, ω_I are given in table 1), where F is defined as in equation (3.5) and K is obtained from the equation of the flow parallel to a cylinder (i.e. approximation of the cercus). Dashed lines represent estimation of $|F(\omega, r, \omega_S, \omega_I)|$ alone.

over a large range of values and retaining the combination which yielded the lowest residual error (see §2). The agreement between fits and data was very good with an average error less than 10 per cent that corresponds to our estimation of the measurement error (see §2). Our approach also allowed us to estimate the precision with which the constants were determined by the fit (table 1 and figure 2*c*). While values of the reduced constants ω_S and r were unambiguous, we could not determine ω_I with satisfactory precision (table 1).

The reason for the poor estimation of ω_I is that it significantly influences the motion only for frequencies beyond the optimal frequency range (figure 2*a*). Like others, we have not been able to measure hair deflection in this range because the angular displacement is too small to be measured optically and the PIV approach was limited in its sampling rate. Therefore, we obtained only a lower bound for ω_I while arbitrarily large values still yielded a fitting error below our estimated measurement error (see the example of obtained fitting error landscape; figure 2*c* and table 1). Nevertheless, this situation shows that filiform hairs are generally designed so that inertial forces come into play only at relatively high frequencies.

We also observed for both species that ω_S decreases with hair length, making shorter hairs poorer sensors of lower frequencies than longer hairs. From our data, $\omega_S/2\pi$ scales at 51 $(L/1000)^{-1.49}$ Hz for spider hairs and at 60 $(L/1000)^{-1.5}$ Hz for cricket hairs (although values of $\omega_S/2\pi$ are more variable in crickets; table 1). This suggests that the reduced elastic constants of cricket and spider hairs follow similar scaling laws, although more data are necessary to support this conclusion. These scaling functions are also close

to what can be derived (62 $(L/1000)^{-1.46}$ Hz using the Stokes drag force or 96 $(L/1000)^{-1.46}$ Hz using the Oseen drag force) from the existing measurements of the absolute mechanical parameter S [12].

Finally, we observed that the reduced damping constant r was close to 0 for longer hairs and tended to increase for shorter hairs both in spiders and crickets. Importantly, the lower bound estimate for r was lower than 1 for all hairs except one. This shows that, as a general rule for both cricket and spider hairs, damping is stronger in air than in the articulation. We have seen that the limit of energy transmission is reached when damping in air and in the articulation are balanced. We observed that this is not exactly the case for the hairs we measured. On the contrary, weak damping in the basal articulation tends to bring a number of hairs, in particular the longest, close to the physical limit of motion near their natural frequency. These results contrast with the conclusions drawn by Shimozawa *et al.* [12] who suggested that hairs of all lengths are optimized for energy transmission. The discrepancy is very likely owing to a not sufficiently precise determination of hair mechanical parameters by these authors (see §4).

The general design of a filiform hair is therefore the combination of a relatively soft articulation with a relatively low inertia (mass) leading to a natural frequency surrounded by a large plateau in the higher frequency range. Interestingly, the low amount of damping in the articulation compared with the damping in air suggests that these hairs are optimized towards the physical limits of angular motion rather than energy transmission, at least for longer hairs.

4. DISCUSSION

4.1. Which criterion for mechanical optimization: impedance-matching or maximal possible motion?

We have shown that energy transmission is as large as physically possible at the natural frequency if the ratio r of damping in the articulation to damping in air is equal to 1, whereas motion requires $r = 0$ to reach its physical limit. We measured this quantity for cricket and spider hairs and found values of r between 0 and 1, with a trend towards smaller r for longer hairs. Hence, there is no uniform optimization for all filiform hairs. The number of hairs presently analysed is too low to distinguish between the following two possibilities: (i) there is a compromise between the two optimization criteria, energy and motion, or (ii) the hair population is heterogeneous with respect to the optimization criteria. This is a fascinating area for further research, in particular, because cricket cercal hairs become longer in successive cricket instars [21] and hairs differing in length are typical of many arrays of spider trichobothria [1].

Longer hairs receive more kinetic energy than shorter hairs because of their larger interaction surface with the airflow. This explains why the limit for transmitted energy increases with hair length (see equation (3.4)). It also suggests that shorter hairs are more constrained by limitations in energy transmission, which is in agreement with their higher r values. We should, however, recall that maximizing energy transmission will only optimize signal transmission in the case of passive elements. The action potential generation mechanism in the sensory neurons is an active process powered by cellular metabolism. Therefore, the sensory information from filiform hairs also goes through at least one active transduction step. What matters in the end is the efficient transmission of information to the nervous system [8,22–24], which is an issue that should be further addressed in the light of our results using electrophysiological recordings.

4.2. Hairs are mechanically optimal at unexpectedly high frequencies

The tuning of filiform hairs is broad in both the spider and the cricket. However, all previous works have considered that the frequency at which the angular displacement is maximal was most representative of the signals for which the hair is tuned. Remarkably, we found that the frequency at which the angular displacement is largest (often described as the resonant frequency) is suboptimal regarding the absolute physical limits (figures 2 and 4*a*,*b*). Our observation relates to previously made observations which showed that the best frequencies of a hair calculated for maximum deflection are clearly lower than those calculated as the ratio of the maximal hair-tip deflection to the maximal displacement of the oscillating air [1]. This study shows where the hairs work at the physical limit. The maximum angular displacement of hairs results from the interplay between the physical limit of angular displacement which behaves as a low-pass filter (figure 4*a*), and the effect of the boundary layer $|K|$, which behaves as a high-pass filter (e.g. compare the dashed and solid red lines in figure 4*a*). This was noticed cursorily by Shimozawa *et al.* [12] but is particularly evident in our new formulation, where the boundary layer effect and the mechanical response are multiplicative. We here suggest that the natural frequency is also an important characteristic frequency, representing the range of signals for which the hair works closest to its physical limit. Importantly, our results do not imply that the underlying sensory neuron is most sensitive at the natural frequency. If the transduction of motion into action potentials follows the angular displacement, the sensory neuron will be maximally sensitive at the frequency for which angular displacement is maximal and not at the natural frequency. However, even in this case, our conclusion that the mechanical sensitivity of the sensor at the natural frequency could hardly be improved by any other passive mechanical design of the hair and that it is in this range of frequencies where the sensor captures the maximum of the physically available signal remains valid.

This raises the question as to whether this system is the only 'design' possible or whether alternatives are also possible. It is straightforward to show that a strongly resonant hair would have its maximum angular displacement at its natural frequencies (figure 4*a*,*b*, black lines). Therefore, a resonant hair would show a larger response than a typical filiform hair at the frequency of maximum angular displacement. For example, a resonant hair could be obtained by increasing inertia and/or making the articulation stiffer (figure 4*c*).

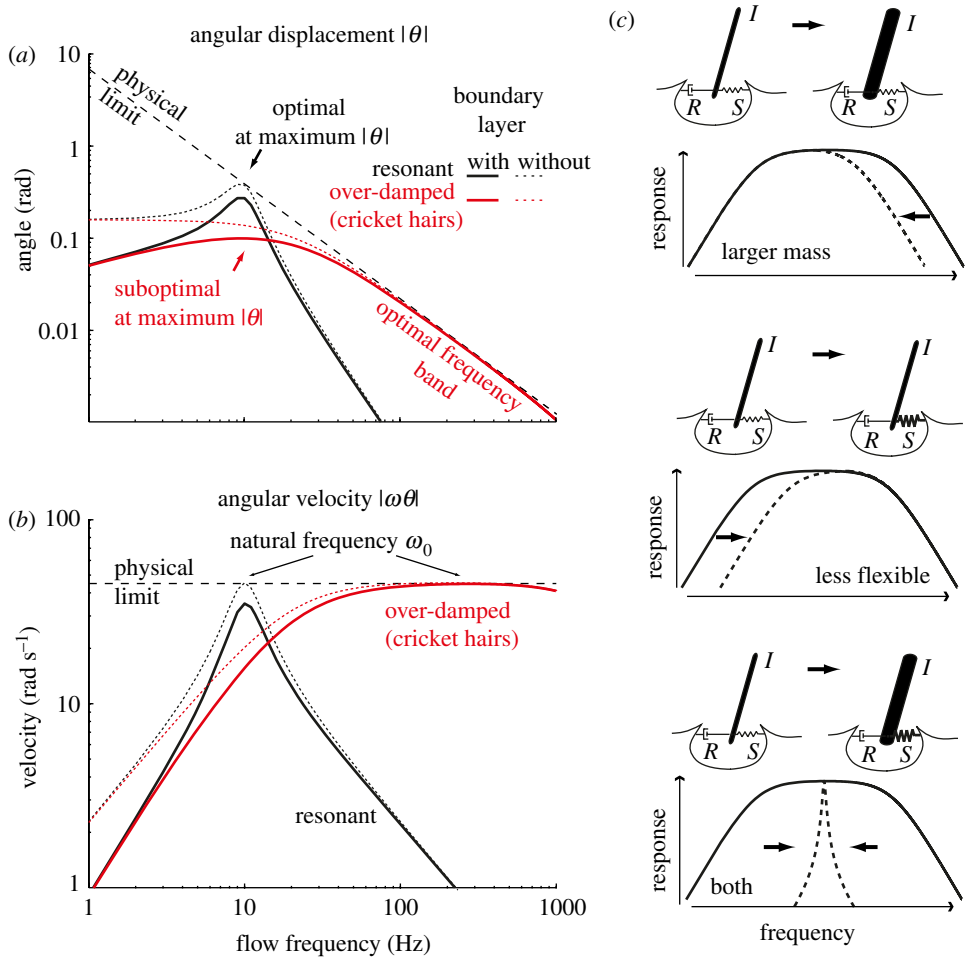

Figure 4. Mechanical optimization of filiform hairs. (*a*,*b*) Filiform hairs (e.g. red line) are over-damped oscillators and are not mechanically optimal at the maximum of their angular displacement (here approx. 10 Hz). As a consequence, it is possible to find a different hair design which is more efficient at this frequency. For example, a strongly resonant hair (e.g. black line) which is closest to optimality at the maximum of its angular displacement (approx. here also 10 Hz) clearly outperforms the filiform hair at approximately 10 Hz. Note that no other design could outperform the filiform hair in the range of frequencies where it works at the physical limit. (*c*) Top: an increase of hair mass leads to a decrease of the high-cut boundary of the optimal frequency band. Middle: an increase in articulation flexibility leads to an increase of the low-cut boundary of the optimal frequency band. Bottom: heavier and less flexible hairs can become mechanically resonant.

However, thicker and heavier hairs would have larger inertias (i.e. lower reduced constant ω_I), which would make them less sensitive to high frequencies (figure 4*c*). On the contrary, one of the most distinctive characteristics of filiform hair design is their extremely small diameter which seems to have no other role than to increase their sensitivity to high frequencies beyond the best frequency where displacement is maximal. The same reasoning might explain why the filiform hairs of the spider *C. salei* have a feathery structure [1]. By decreasing the mass of the hairs, this structure reduces their inertia considerably, while increasing the friction in air [1,10]. The combination of these two properties strongly increases the sensitivity to high frequencies by increasing ω_I. It should be noted that resonant hairs are also slower to reach their steady state response, which would contrast with the clearly phasic properties of the entire wind-sensing system, as evidenced from electrophysiological and biomechanical experiments [3,14,16,25].

Therefore, it seems that the 'design' of filiform hairs evolved to maximize mechanical sensitivity to higher frequencies (or equivalently the sensitivity to fast signals, such as transient and fast fluctuations), rather than to optimize the response at the frequency where the angular velocity is maximal. From an evolutionary point of view, this suggests the existence of strong pressures selecting for high sensitivity at higher frequencies.

4.3. Conflicting results regarding parameter estimation in previous reports

Previous reports have readily provided estimates of the spider and cricket mechanical parameters, by fitting the hair motion model to experimental data of hair angular displacement. The most complete set of mechanical parameters for cricket filiform hairs is found in Shimozawa *et al.* [12]. Estimates have also been published for the spider [10,11]. Despite the similarity of the estimation method, we found some significant discrepancies in our new results.

A first interesting discrepancy is that according to Shimozawa *et al.*, filiform hairs of the cricket *Gryllus bimaculatus* are working close to optimal energy transmission (impedance-matching) because they found

that $R \sim R_\mu$, or equivalently that $r \sim 1$. However, this conclusion depends on the estimate of R_μ that Shimozawa *et al.* [12] chose for their theoretical fits. We obtained $r = 0.23\ (L/1000)^{-0.48}$ when we used scaling functions for R and R_μ obtained by Shimozawa *et al.* [12] based on Oseen's theory and $r = 1.46\ (L/1000)^{-0.23}$ when we used their estimate based on Stokes' theory. Hence, the estimate based on Oseen's theory indicates that hairs are close to optimal motion (r close to 0), while the estimate based on Stokes' theory puts them far from optimal motion. Our results clearly indicate that r is biased towards 0, at least for the longer hairs studied here. We noticed that the theoretical fit to the data using Stokes' theory provided by Shimozawa *et al.* [12] is particularly poor for longer hairs in the range of the natural frequency. Interestingly, it is around the natural frequency that r most strongly affects the response of the hair. Most likely then, the observed discrepancy between the theoretical fit and the data at these frequencies explains the inaccuracy of estimates of r by Shimozawa *et al.* [12].

A second difference from the literature is that according to our present results, both cricket and spider hairs are over-damped, with values for the damping ratio ζ between 1 and 2. This is consistent with values derived by Shimozawa *et al.* for the cricket, but some studies suggested that spider hairs are resonant [10,18], although even the shape of the tuning curves first obtained [1] showed rather broad peaks only. We think that the latter conclusion was erroneously drawn from an overestimation of the inertia of spider hairs. Interestingly, the theoretical fit to angular displacement data from spider trichobothria also displays stronger inaccuracies in the range of the natural frequency of the hair (i.e. beyond the frequency at which the displacement of the hair is maximum).

4.4. Broadband tuning and lower frequencies' attenuation

The large ζ values that we observe imply a large breadth of tuning around the natural frequency of the hair, which make the mechanical response of filiform hairs behave as typical broadband receptors in the higher frequency range as we observe in our measurements (figures 2 and 3). As mentioned earlier, the higher frequency cut-off of the optimal frequency range is set by inertia. The low frequency cut-off (in the absence of boundary layer effects which play a much less important role with regard to the natural as opposed to the 'best frequency' discussed in the existing literature) is mainly set by the stiffness of the articulation via ω_S (figures 1*d* and 4*c*), because the elastic forces in the articulation are the dominant factors for the attenuation of low frequencies (figure 1). Two hydrodynamic mechanisms work in the same direction as the elasticity of the articulation. The first one is the attenuation of the incoming airflow by the substrate (figure 1*c*). The second one is hair-to-hair interactions. Filiform hairs often come alone or in groups with distances being large relative to hair diameter and therefore not affecting each other. On the insect cercus, they are found in high densities. The hydrodynamic interactions between neighbouring hairs, the so-called viscous coupling effects, are frequency dependent [9,26,27]. They tend to vanish at high frequencies. In addition, viscous interactions are minimized near the natural frequency, because hairs have minimal influence on the flow at this frequency [9,27]. Hence, viscous interactions, where present, should result in an increased attenuation of lower frequencies, thereby enhancing the contrast between low and high frequencies. Thus, having closely spaced arrangements of filiform hairs like those on the cricket cercus could represent an original design for the improved identification of high-frequency components of ecologically relevant signals.

4.5. Beware the approaching object

Natural airflows are often broadband, with most energy located in the lower frequencies [6,8,14,28]. This is particularly true for signals of abiotic origin, such as wind turbulence near the ground [29], but biologically relevant signals also have strong low-frequency components [8,14]. The fact that larger angular displacements (however suboptimal) are observed at lower frequencies might reflect a compromise between obtaining the maximum possible sensitivity at higher frequencies and keeping a good sensitivity at lower frequencies. (Note that air particle displacement decreases with flow frequency when flow energy is kept constant.) This suggests that the design of filiform hairs was selected to allow reception of a large variety of signals with different energies and frequencies. Because of the relatively weak energy of high frequencies in natural signals, one might simply assume that their uptake and detection require more physical perfection of the sensor than do low frequencies. A number of studies have also pointed out that biologically relevant airflows are specific in that they contain fast fluctuations or transients, and frequencies higher than those typical of background noise [3]. An approaching object produces a ramp-like signal, as proposed on theoretical grounds and cursorily observed for a predatory wasp approaching a cricket or a toad eating a cricket [15,30]. A quantitative characterization of such a signal was carried out by Casas *et al.* [7], who recorded the airflow signals in front of running wolf spiders, a major predator of this cricket species [31]. At the rear of the cricket, the airflow intensity increases in a cubic fashion until capture. This type of signal, analysed in terms of frequency content, shows an increasing proportion of high-frequency signals over time. This is true irrespective of the locomotion mode of the moving animal (e.g. running or flying). A predatory spider running towards an unwary cricket and a fly flying towards a stationary alert predatory spider produce signals in which the progressively increasing amount of higher frequency airflows signify imminent encounter [3,14]. The filiform hairs of prey and predator arthropods may have attained the mechanical response properties close to the physical limit over the course of evolution to precisely assess such close encounters. In addition, the fractionation of hair length associated with shifts of the band of mechanically optimal frequencies found in the arrays of both spider trichobothria and cricket cercal hairs (figures 2 and 3) suggests that these animals are interested in perceiving a relatively broad band of frequencies, from as low as 40 Hz to potentially several hundred hertz (table 1).

As has been suggested in earlier studies when considering the shifts in frequency of maximal angular displacement according to hair length [1,12,13], the biologically relevant high-frequency content of airflows can be properly signalled by a gradual recruitment of hairs of different length, the shortest ones being mechanically optimal for the highest frequency range.

We are grateful to O. Dangles for helpful discussions. B.B. acknowledges support from the Ecole Normale Supérieure (Paris) which made his stay in the laboratory of F.G.B. possible and from the International Human Frontier Science Programme Organization for current funding. B.B., J.C. and F.G.B. designed the research, B.B. performed the theoretical analysis, B.B. and T.S. performed the experiments, and B.B., T.S., J.C. and F.G.B. wrote the manuscript.

REFERENCES

1 Barth, F. G., Wastl, U., Humphrey, J. A. C. & Devarakonda, R. 1993 Dynamics of arthropod filiform hairs. II. Mechanical properties of spider trichobothria (*Cupiennius salei* Keys). *Phil. Trans. R. Soc. Lond. B* **340**, 445–461. (doi:10.1098/rstb.1993.0084)

2 Casas, J. & Dangles, O. 2010 Physical ecology of fluid flow sensing in arthropods. *Annu. Rev. Entomol.* **55**, 505–520. (doi:10.1146/annurev-ento-112408-085342)

3 Barth, F. G. 2002 Spider senses: technical perfection and biology. *Zoology* (*Jena*) **105**, 271–285. (doi:10.1078/0944-2006-00082)

4 Brittinger, W. 1998 Trichobothrien, Medienströmung und das Verhalten von Jagdspinnen (*Cupiennius salei*, Keys). Doctoral thesis, University of Vienna, Austria.

5 Klopsch, C., Humphrey, J. A. C. & Barth, F. G. 2007 The air flow generated by a flying prey insect around a wandering spider and its motion sensing hair sensilla. In *5th Int. Symp. on Turbulence and Shear Flow Phenomena*, pp. 1023–1028. Munich, Germany: Technical University of Munich.

6 Barth, F. G., Humphrey, J. A. C., Wastl, U., Halbritter, J. & Brittinger, W. 1995 Dynamics of arthropod filiform hairs. III. Flow patterns related to air movement detection in a spider (*Cupiennius salei* Keys). *Phil. Trans. R. Soc. Lond. B* **347**, 397–412. (doi:10.1098/rstb.1995.0032)

7 Casas, J., Steinmann, T. & Dangles, O. 2008 The aerodynamic signature of running spiders. *PLoS ONE* **3**, e2116. (doi:10.1371/journal.pone.0002116)

8 Rinberg, D. & Davidowitz, H. 2003 Wind spectra and the response of the cercal system in the cockroach. *J. Comp. Physiol. A* **189**, 867–876. (doi:10.1007/s00359-003-0460-9)

9 Bathellier, B., Barth, F. G., Albert, J. T. & Humphrey, J. A. C. 2005 Viscosity-mediated motion coupling between pairs of trichobothria on the leg of the spider *Cupiennius salei*. *J. Comp. Physiol. A* **191**, 733–746. (doi:10.1007/s00359-005-0629-5)

10 Humphrey, J. A. C. & Barth, F. G. 2008 Medium flow-sensing hairs: biomechanics and models. *Adv. Insect Physiol. Insect Mech. Control* **34**, 1–80. (doi:10.1016/S0065-2806(07)34001-0)

11 Humphrey, J. A. C., Devarakonda, R., Iglesias, I. & Barth, F. G. 1993 Dynamics of arthropod filiform hairs. I. Mathematical modelling of the hair and air motions. *Phil. Trans. R. Soc. Lond. B* **340**, 423–444. (doi:10.1098/rstb.1993.0083)

12 Shimozawa, T., Kumagai, T. & Baba, Y. 1998 Structural scaling and functional design of the cercal wind-receptor hairs of cricket. *J. Comp. Physiol. A* **183**, 171–186. (doi:10.1007/s003590050245)

13 Shimozawa, T. & Kanou, M. 1984 Mechanical properties and angle thresholds of cercal filiform sensilla of a cricket. *Zool. Sci.* **1**, 868.

14 Barth, F. G. & Höller, A. 1999 Dynamics of arthropod filiform hairs. V. The response of spider trichobothria to natural stimuli. *Phil. Trans. R. Soc. Lond. B* **354**, 183–192. (doi:10.1098/rstb.1999.0370)

15 Camhi, J. M., Tom, W. & Volman, S. 1978 The escape behavior of the cockroach *Periplaneta americana*. II. Detection of natural predators by air displacement. *J. Comp. Physiol. A* **128**, 203–212.

16 McConney, M. E., Schaber, C. F., Julian, M. D., Eberhardt, W. C., Humphrey, J. A. C., Barth, F. G. & Tsukruk, V. V. 2009 Surface force spectroscopic point load measurements and viscoelastic modelling of the micromechanical properties of air flow sensitive hairs of a spider (*Cupiennius salei*). *J. R. Soc. Interface* **6**, 681–694. (doi:10.1098/rsif.2008.0463)

17 Panton, R. I. 1984 *Incompressible flow*. New York, NY: Wiley.

18 Kant, R. & Humphrey, J. A. C. 2009 Response of cricket and spider motion-sensing hairs to airflow pulsations. *J. R. Soc. Interface* **6**, 1047–1064. (doi:10.1098/rsif.2008.0523)

19 Steinmann, T., Casas, J., Krijnen, G. & Dangles, O. 2006 Air-flow sensitive hairs: boundary layers in oscillatory flows around arthropod appendages. *J. Exp. Biol.* **209**, 4398–4408. (doi:10.1242/jeb.02506)

20 Bialek, W. 1987 Physical limits to sensation and perception. *Annu. Rev. Biophys. Biophys. Chem.* **16**, 455–478. (doi:10.1146/annurev.bb.16.060187.002323)

21 Dangles, O., Pierre, D., Magal, C., Vannier, F. & Casas, J. 2006 Ontogeny of air-motion sensing in cricket. *J. Exp. Biol.* **209**, 4363–4370. (doi:10.1242/jeb.02485)

22 Jacobs, G. A., Miller, J. P. & Aldworth, Z. 2008 Computational mechanisms of mechanosensory processing in the cricket. *J. Exp. Biol.* **211**, 1819–1828. (doi:10.1242/jeb.016402)

23 Levi, R. & Camhi, J. M. 2000 Population vector coding by the giant interneurons of the cockroach. *J. Neurosci.* **20**, 3822–3829.

24 Theunissen, F., Roddey, J. C., Stufflebeam, S., Clague, H. & Miller, J. P. 1996 Information theoretic analysis of dynamical encoding by four identified primary sensory interneurons in the cricket cercal system. *J. Neurophysiol.* **75**, 1345–1364.

25 Friedel, T. & Barth, F. G. 1997 Wind-sensitive interneurons in the spider CNS (*Cupiennius salei*). Directional information processing of sensory inputs from trichobothria on the walking legs. *J. Comp. Physiol. A* **180**, 223–233. (doi:10.1007/s003590050043)

26 Casas, J., Steinmann, T. & Krijnen, G. 2010 Why do insects have such a high density of flow-sensing hairs? Insights from the hydromechanics of biomimetic MEMS sensors. *J. R. Soc. Interface* **7**, 1487–1495. (doi:10.1098/rsif.2010.0093)

27 Lewin, G. C. & Hallam, J. 2010 A computational fluid dynamics model of viscous coupling of hairs. *J. Comp. Physiol. A* **196**, 385–395. (doi:10.1007/s00359-010-0524-6)

28 Rinberg, D. & Davidowitz, H. 2000 Do cockroaches 'know' about fluid dynamics? *Nature* **406**, 368. (doi:10.1038/35019161)

29 Finnigan, J. 2000 Turbulence in plant canopies. *Annu. Rev. Fluid Mech.* **32**, 519–571. (doi:10.1146/annurev.fluid.32.1.519)

30 Gnatzy, W. 1996 *Digger wasp vs. cricket: neuroethology of a predator–prey interaction*. Stuttgart, Germany: Fischer.

31 Dangles, O., Casas, J. & Coolen, I. 2006 Textbook cricket goes to the field: the ecological scene of the neuroethological play. *J. Exp. Biol.* **209**, 393–398. (doi:10.1242/jeb.02000)